I.A.U
Karaj branch

Journal of
A p p l ied
C hemical
R esearch
jacr.kiau.ac.ir

Journal of Applied Chemical Research, 18, 4, 40-55 (2024)

Detection of Nitrofurantoin using a Modified Glassy Carbon Electrode with Woolen Ball-shaped La^{3+}/TiO_2 Nanostructure as a Sensitive Electrochemical Sensor

Mohammad Mehdi Foroughi[*,1], Shohreh Jahani[2], Soroush Rashidi[3], Mehran Moradalizadeh[1]

[1]*Department of Chemistry, Kerman Branch, Islamic Azad University, Kerman, Iran*

[2]*Bam University of Medical Sciences, Bam, Iran*

[3]*Department of Civil Engineering, Islamic Azad University, Kerman, Iran*

(Received 18 Feb. 2024; Final revised received 12 May 2024)

Abstract

Specialists in disease diagnosis and biomedical chemistry have always sought to detect a variety of antibiotics, such as nitrofurantoin (NFT) in various matrices. The current attempt was also made to detect NFT in phosphate buffer solution using a glassy carbon electrode modified with as-fabricated woolen ball-shaped La^{3+}/TiO_2 nanostructure (WB-S La^{3+}/TiO_2-NS/GCE) according to techniques of cyclic voltammetry, chronoamperometry and differential pulse voltammetry. The effects of WB-S La^{3+}/TiO_2-NS result in an electrocatalytic-type response providing a significantly improved electroanalytical response compared to a bare unmodified GCE. The produced sensor was also strong in studying the concentration changes of NFT, with the limit of detection of 0.57 nM. Moreover, the proposed sensor was successful in sensing the NFT in real specimens, and exhibited appreciable stability and repeatability.

Keywords: Nitrofurantoin, Voltammetry, Lanthanum, Nanostructure, Titanium dioxide.

****Corresponding author**: Mohammad Mehdi Foroughi, Department of Chemistry, Kerman Branch, Islamic Azad University, Kerman, Iran. Email: foroughi@iauk.ac.ir, Foroughi@iauk.ac.ir.*

Introduction

Nitrofurans are known as broad-spectrum veterinary antibiotics, which are extensively consumed for farming cattle, swine, poultry, bee, shrimp and fish [1]. The use of these synthetic antibiotics, a characteristic structural 5-membered nitrofuran, is as feed additives to enhance growth, curative and preventive therapy of protozoal and bacterial infections [2].

The recent findings of medical research underlined a strong carcinogenic effect of nitrofurans especially due to the risk of significant residues in meat, honey, milk and other foods of animal origin [3,4]. The agricultural use of nitrofurans has been banned in numerous countries due to the potential risks to human health. However, due to low production cost and excellent efficacy, this group of antibiotics is still used on a large scale around the world, especially in developing countries. Harmful effects of veterinary antibiotic residues on human health make analytical control of these drugs necessary to ensure consumer protection [5-7].

Hence, it is vital to quantify the amount of nitrofurans through sensitive and facile analytical techniques for pollution control; some of these methods are flame atomic fluorescence spectrometry, atomic absorption spectrophotometry, plasma atomic emission spectrometry and capillary electrophoresis [8-14]. Despite many advantages of such analytical techniques, there are several disadvantages for them, such as time-consuming, expensive equipment and need for difficult operations. Among these, electrochemical approaches attracted further attention for the analysis of trace contaminants [15,16].

The working electrode is employed to investigate the detection efficiency of an electrochemical sensor. The place of mass and electron transfer is the interface between the solution and the working electrode. Electrode materials with high electrical conductivity and great catalytic performance are required, which needs great sensitivity and rapidity of a sensor, and can be realized through diverse modified electrodes to catalyze electrode reactions [17]. Modifiers with appreciable features, including great conductivity, excellent catalytic performance and large active area, can achieve the electrode surface modification. It would be very beneficial to develop electrochemically modified materials and techniques for clinical trials and forensic applications of analytes [18,19].

TiO_2 as one of the effective electrocatalyst has broad bandgap, high chemical stability, low cost and excellent catalytic profile. TiO_2 nanoparticles (NPs) accelerate electrolysis and electron transfer because of large electroactive surface area, which depends on their structure, shape and size [20,21]. Further active sites and carriers for the redox process are found on the TiO_2 surface doped with rare earth metal [22]. The element lanthanum (La) has been previously analyzed as the dopant for TiO_2 electrocatalyst [23]. The dopant La could reportedly enhance the anatase phase stability and prevent the crystal growth at high temperature [24,25].

The present attempt was made to fabricate woolen ball-shaped La^{3+}/TiO_2 nanostructure (WB-S La^{3+}/TiO_2-NS), followed by characterization using techniques of X-ray diffraction (XRD), scanning electron microscopy (SEM) and energy-dispersive X-ray spectroscopy (EDX). A glassy carbon electrode (GCE) was then surface modified with WB-S La^{3+}/TiO_2-NS (WB-S La^{3+}/TiO_2-NS/GCE) to detect nitrofurantoin (NFT). The sensor was examined to detect NFT in pharmaceutical matrix and human urine specimens, the results of which highlighted appreciable recoveries, with good relative standard deviation (RSD), superior reproducibility and repeatability.

Experiments

Chemicals and devices

A SAMA 500 Electro analyzer was utilized to carry out all electrochemical tests. We employed a routine three-cell electrochemical system, including unmodified (bare) and modified glassy carbon working electrode, a reference electrode of Ag/AgCl (vs. 3.0 M KCl), and an auxiliary electrode of platinum wire. The solution pH was adjusted by a digital pH meter (Corning, Model: 140) equipped with a glass electrode (alongside an Ag/AgCl reference electrode, Model: 6.0232.100). A Philips analytical PC-APD X-ray diffractometer equipped with a graphite monochromatic Cu (α_1, λ_1=1.54056 Å) and Kα (α_2, λ_2=1.54439 Å) radiation was recruited to record X-ray powder diffraction (XRD) to monitor the product organization. A KYKY and EM 3200scanning electron microscopy (SEM) was used to explore the morphology of nanostructure. EDX spectroscopy is an example of a non-destructive instrument used for analysis, such as the analysis of chemical compounds. The buffered solution pH was adjusted by a digital Ion Analyzer 250pH meter (Corning) with precision of ±0.001.

Nitrofurantoin (>99.0%) with very high purity belonged to Merck Company. Glacial acetic acid, titanium butoxide, lanthanum chloride, absolute ethanol and NaOH with analytical grade with no need for additional purification belonged to Sigma-Aldrich Company. Na_2HPO_4 (0.1 M) and NaH_2PO_4 (0.1 M) at various ratios were used to prepare the phosphate buffer solutions (PBS). H_3PO_4 (1.0 M) and/or NaOH were used to adjust the solution pH.

Fabrication of Woolen ball-shaped La^{3+}/TiO_2 nanostructure (WB-S La^{3+}/TiO_2-NS)

Titanium butoxide (1 mL) and the solution of lanthanum chloride (0.02 g) in 1 mL distilled water were appended drop-by-drop into glacial acetic acid (30 mL) while stirring continuously for 10 min at an ambient temperature to obtain white suspension, which was then positioned in a 150-mL Teflon-lined autoclave at 140 °C for 12 h. The appeared white product was gathered by

centrifugation, rinsed several times initially with Milli-Q and then with ethanol, and finally dried in a 60-°C oven overnight to obtain as as-fabricated WB-S La^{3+}/TiO_2-NS.

Synthesis of WB-S La^{3+}/TiO_2-NS electrode

Considering the significance of electrode fabrication in electrochemistry, first the glassy carbon electrode (GCE) surface was completely rinsed with water to get rid of possible impurities. The following protocol was implemented to prepare the WB-S La^{3+}/TiO_2-NS/GCE. First, WB-S La^{3+}/TiO_2-NS suspension was synthesized by dispersing WB-S La^{3+}/TiO_2-NS (1 mg) in double distilled water (1 mL) under 30-min sonication. Then, WB-S La^{3+}/TiO_2-NS suspension (6 µL) was drop coated on the surface of GCE and dried at the ambient temperature.

Preparation of real specimens

NFT tablets (labeled 100 mg NFT/tablet) were powdered, 100 mg of which was then appended into water (25 mL) and exposed to ultra-sonication. A certain volume of the obtained solution alongside phosphate buffer solution (PBS, pH 7.0) was water-diluted in a 10-mL voltammetric flask. The achieved solution was applied for the NFT analysis.

Blood samples gathered in heparinized test tubes underwent a centrifugation for 10 min at 3000 rpm to separate the plasma, which was then refrigerated for next testing. Acetonitrile was used to deprotonate the plasma samples, so that the acetonitrile (2 mL) was appended to plasma and the mixture underwent a centrifugation for 10 min at 2000 rpm. The supernatant was evaporated in a conical flask to dryness in exposure to nitrogen flow. The dry residue was diluted with PBS (pH 7.0) and poured into the voltammetric cell (20 mL) for analysis with no need for pretreatment. The NFT were quantified in the samples according to standard addition method.

Urine specimens sampled from healthy subjects were analyzed to determine possible traces of NFT. After that, the samples were diluted 50 times with PBS to avoid the matrix effect of valid samples.

Results and discussion

Determination of WB-S La^{3+}/TiO_2-NS characteristics

The XRD patterns captured from pure TiO_2 (curve a) and La^{3+}/TiO_2 nanostructure (curve b) are presented in Figure 1. Crystal structures of pure TiO_2 and nanostructured La^{3+}/TiO_2 were mainly composed of anatase phase (JCPDS 21-1272). The anatase peaks appeared at 25.371, 38.51, 48.211, and 54.101 were related to (101), (004), (200), and (105) planes, sequentially. There were no distinct peaks (La^{3+} metal, La_2O_3) following the integration of La dopants into the TiO_2 nanostructure probably due to inadequate sensitivity of XRD analysis in sensing traces of La dopants within the TiO_2 nanostructure [26]. The shift of diffraction peaks and the change in full width at half maximum for the La^{3+}/TiO_2 nanostructure, anatase phase may be attributed to the integration of La^{3+} dopants into the TiO_2 lattice.

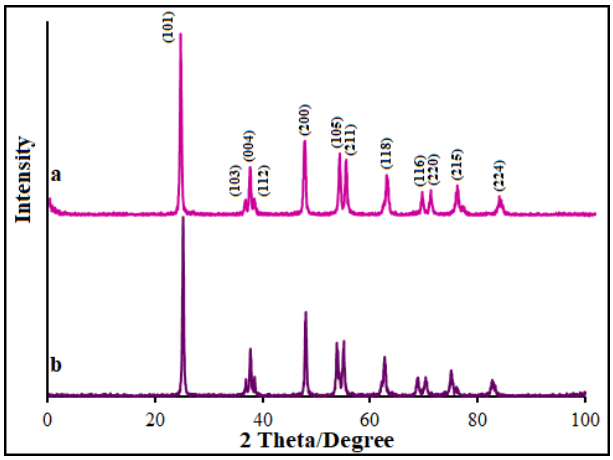

Figure 1. XRD pattern of a) A-L TiO_2 NF and b) WB-S La^{3+}/TiO_2-NS.

The FE-SEM images (Figure 2a, b) were applied to explore the morphology of Anatase-like TiO_2 nanoflowers (A-L TiO_2 NF), the findings of which clarified a spherical hierarchical architecture with thin and long two-dimensional nanosheets (i.e., ~10-nm petals, forming A-L TiO_2 NF) protruding from the center of the three-dimensional nanoflowers (2-6 µm in diameter, the mean diameter of 4.5 µm). Based on Figure 2c, as-produced woolen ball-shaped La^{3+}/TiO_2 nanostructures (WB-S La^{3+}/TiO_2 NS) consisted of large-scale woolen ball-flower structures (1.8 to 2.4 mm in diameter). SEM images with high magnification from WB-S La^{3+}/TiO_2 NS (Figure 2d) present two-dimensional well-ordered and -oriented nanoplates (20-30 nm) for WB-S La^{3+}/TiO_2 NS to form woolen ballflower structures. The FE-SEM images exhibits the impact of La ion content on the TiO_2 morphology.

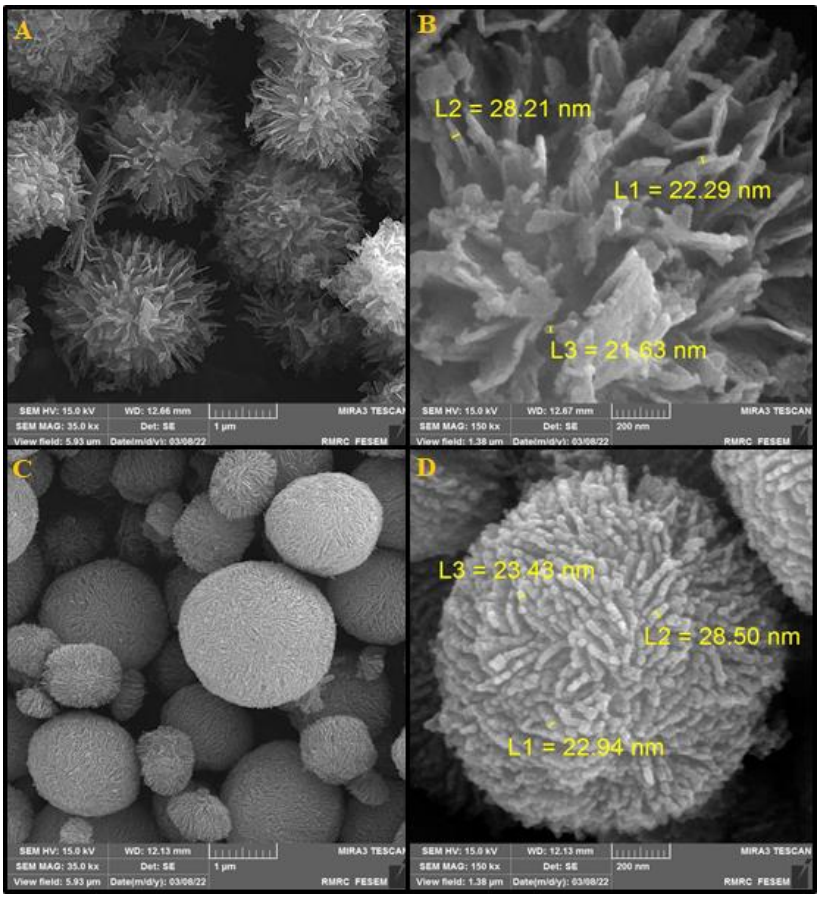

Figure 2. (A) FESEM image (B) High resolution FESEM image of A-L TiO_2 NF. (C) FESEM image (D) High resolution FESEM image of WB-S La^{3+}/TiO_2-NS.

The EDS pattern (Figure 3) shows that the woolen ballflower products are built of Ti, O and La elements without any impurity. The distribution of Ti, O and La was confirmed by the elemental mapping.

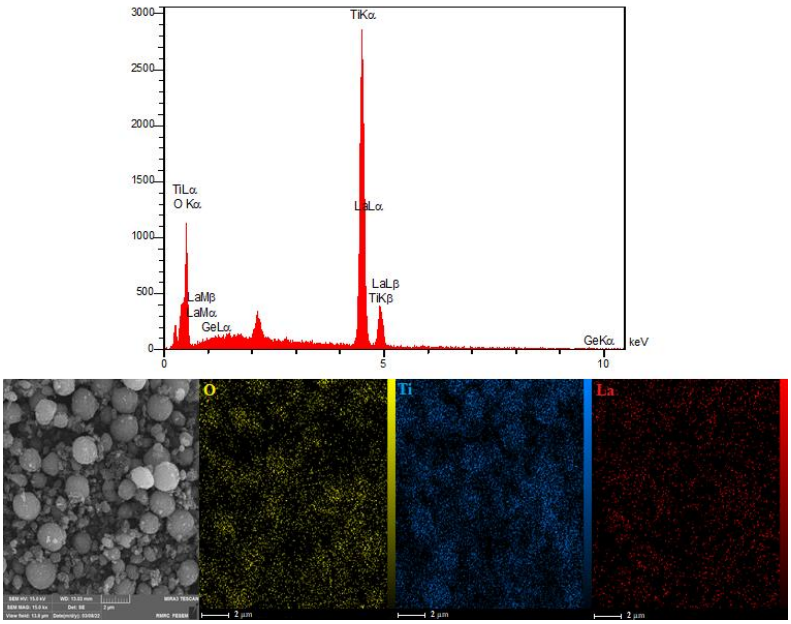

Figure 3. EDX spectra and elemental mapping of WB-S La^{3+}/TiO_2-NS.

Electrochemical behavior of NFT on the modified electrode

The electrochemical response of NFT (100.0 µM) was recorded in PBS (pH 7, 0.1 M) at scan rate of 50 mV/s using the CVs on bare GCE (curve a), A-L TiO_2 NF/GPE (curve b) and WB-S La^{3+}/TiO_2-NS/GCE (curve c) (Figure 4). The peak current of NFT reduction had a significant elevation approximately 1.26 and 6.45 times higher on the WB-S La^{3+}/TiO_2-NS/GCE than that on the A-L TiO_2 NF/GCE and bare GCE, sequentially. The peak potentials of them were switched to less positive side with WB-S La^{3+}/TiO_2-NS/GCE than A-L TiO_2 NF/GCE and bare GCE, sequentially. The peak potential was seen for NFT at -0.45 V on the WB-S La^{3+}/TiO_2-NS/GCE and A-L TiO_2 NF/GCE, at -0.51 V on a bare GCE, sequentially, highlighting a platform role of both La^{3+} and TiO_2 electrodes for the NFT reduction.

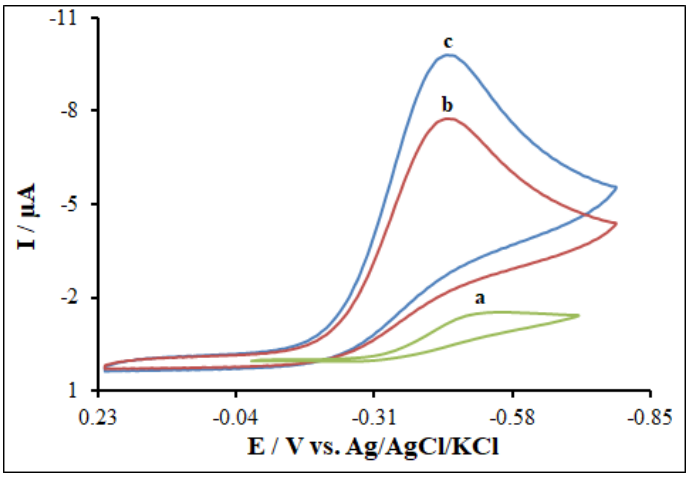

Figure 4. CVs of NFT (100.0 µM) at a) bare GCE, b) A-L TiO_2 NF/GCE and c) WB-S La^{3+}/TiO_2-NS/GCE in 0.1 M PBS (pH=7.0).

Additionally, the pH influence was determined in the range of 5 to 9 on the reduction reaction of NFT (70.0 µM) using the WB-S La^{3+}/TiO_2-NS platform at the scan rate of 50 mV/s (Figure 5a). There was a gradual elevation in the anodic peak currents of NFT when the solution pH elevated to 7 from 5, followed by reducing as the solution pH increased by 8. Hence, the optimal pH value was selected to be 7 for next testing, almost near to physiological medium. Further, we evaluated the dependence of the NFT peak potentials to the pH, see Figure 5b. As the pH changes, the peak potentials of NFT shift to the negative side due to the involvement of proton from the reduction of electrolytic molecules. The linear graphs of the changes of the peak potential against the pH values of the solution showed that the slope of the plot was 0.0487. The proximity of these slope values to the Nernstian slope (0.059) indicates the reduction of NFT on the WB-S La^{3+}/TiO_2-NS/GCE, which involve equal numbers of protons and electrons [27]. Therefore, the electrochemical reaction mechanism of NFT reduction on the electrode modified with WB-S La^{3+}/TiO_2-NS is shown in

Scheme 1, in the process of direct conversion of the nitro compound (–NO_2) to the nitroso derivative(–NHOH), 4 electrons, and 4 protons are exchanged [28].

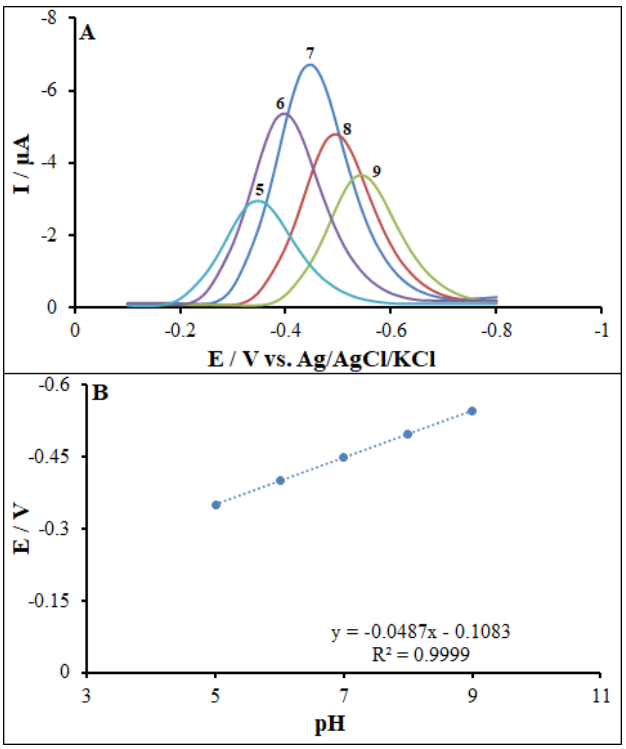

Figure 5. (A) Effect of pH on the peak currents for the reduction of AA (70.0 µM) pH= 5-9. (B) Plots of peak potential vs. pH. Scan rate: 50 mV/s.

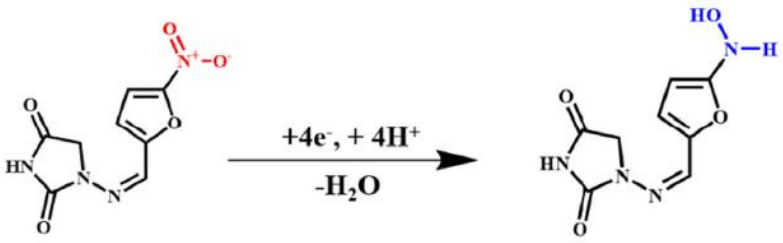

Scheme 1. The electrochemical mechanism of NFT at modified electrode.

Further, we investigated the influence of the scan rate of the modified electrode system with respect to the reduction of NFT (65.0 µM) in the changes of the scan rate, as shown in Figure 6. There was an elevation in the NFT anodic currents when the scan rate boosted to 700 from 10 mV/s. According to the inset, the liner curves of NFT anodic currents against the scan rate square root ($v^{1/2}$) confirms diffusion-controlled process for the reduction of NFT on the WB-S La^{3+}/TiO_2-NS/GCE.

Since charging current (i_c) is depended to the v and Faraday current is depended to the $v^{1/2}$. Therefore, at higher scan rate the charging current will increase significantly. Therefore, the lower scan rate is used to perform the tests. On the other hand, it takes longer to test at very low scan rate.

According to the above, maintain, for the experiments, the scan rate of 50 mVs^{-1} was chosen as the optimal scan rate.

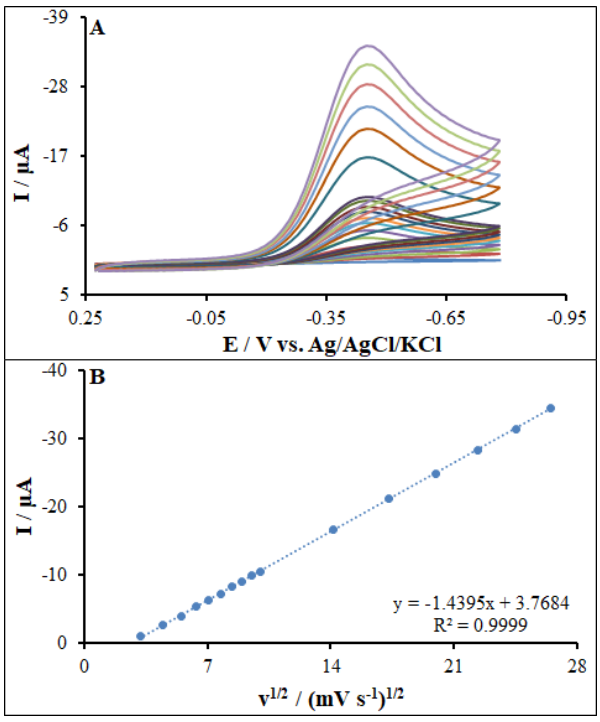

Figure 6. (A) CVs of WB-S La^{3+}/TiO_2-NS/GCE in pH 7.0 in the presence of NFT (65.0 µM) at various scan rates (from inner to outer curve): 10, 20, 30, 40, 50, 60, 70, 80, 90, 100, 200, 300, 400, 500, 600 and 700 mV/s. (B) The plots of peak currents vs. $\upsilon^{1/2}$ of NFT.

Chronoamperometric determinations

The chronoamperometric determination was carried out by altering the level of NFT in PBS at the potentials of 500 mV set for WB-S La^{3+}/TiO_2-NS/GCE (Figure 7A).

The current response (I) for diffusion-controlled process of electroactive NFT was explained by Cottrell's equation (Eq. 1) [27]:

$$I = nFAD^{1/2}C_b\pi^{-1/2}t^{-1/2} \qquad \text{(Eq. 1)}$$

Where, D (cm^2s^{-1}) stands for the diffusion coefficient of studied species, F for the Faraday constant (96485 CM), C_b for the bulk content of studied species (mol cm^{-3}), n for the number of electrons transferred (2), and A for electrode surface area (cm^2). Data revealed a linear curve from the raw chronoamperometric traces for variable NFT levels by diagraming I versus $t^{-1/2}$ (Figure 7B). Then, the slope of the straight lines versus the concentrations of NFT in Figure 7C was drawn. Next, the estimated diffusion coefficient was 3.42×10^{-6} cm^2s^{-1} for NFT.

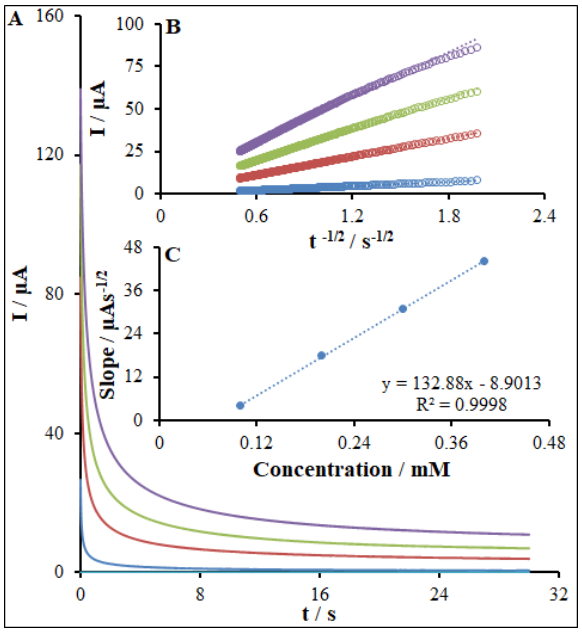

Figure 7. (A) Chronoamperograms obtained at WB-S La^{3+}/TiO_2-NS/GCE in 0.1 M PBS (pH 7.0) for different concentration of NFT. The numbers 1–4 correspond to: 0.1, 0.2, 0.3 and 0.4 mM of NFT. (B) Plots of I vs. $t^{-1/2}$ obtained from chronoamperograms 1-4 for NFT. (C) Plot of the slope of the straight lines against NFT concentration, respectively.

Detection of NFT

The DPVs (Figure 8) were recorded for variable NFT levels in PBS (pH=7, 0.1 M) to determine the performances of WB-S La^{3+}/TiO_2-NS/GCE for the detection of NFT. There was an elevation in the peak currents when the solution level of NFT increased whereas the peak potentials of NFT were constant. The relevant liner standard plots were achieved in the ranges of 0.001 to 500.0 µM for NFT. Linear regression equation of standard graphs and correlation coefficient of NFT are given as follows:

$$I_{NFT} = -0.1001\ C_{NFT} + 0.1213,\ R^2 = 0.9998 \qquad \text{(Eq. 2)}$$

The limit of detection (LOD) of NFT was determined on the basis of five determinations of the blank noise standard deviation (n = 5) on the basis of reported method, using the equation$3S_b/m$; where, m stands for the slope of the standard plot and S_b for the standard deviation, which was 0.57 ± 0.01 µM. The narrow LOD of NFT with as-fabricated nanocomposite suggests good work and efficient analysis of WB-S La^{3+}/TiO_2-NS/GCE.

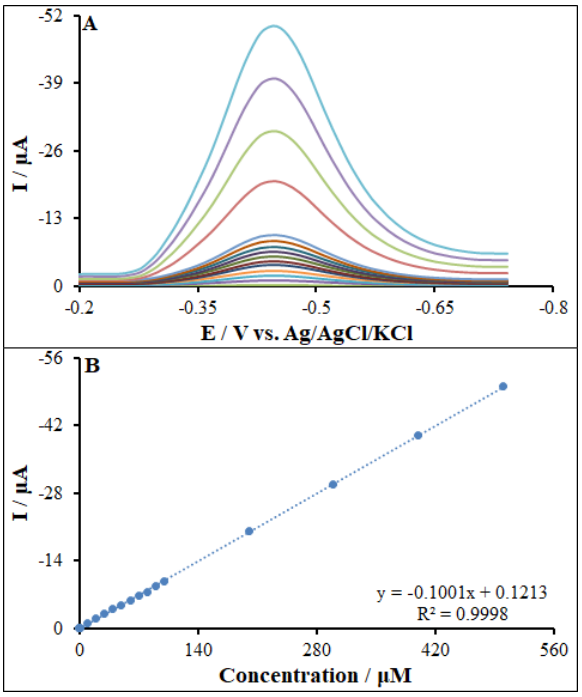

Figure 8. (A) DPVs of the NFT at the WB-S La^{3+}/TiO_2-NS/GCE in PBS (pH 7.0) at the scan rate of 50 mV s^{-1}, respectively, Concentrations from inner to outer of curves: 0.001, 0.1, 1.0, 10.0, 20.0, 30.0, 40.0, 50.0, 60.0, 70.0, 80.0, 90.0, 100.0, 200.0, 300.0, 400.0 and 500.0 µM. (B) Plots of I vs. Concentrations of NFT.

Stability and reproducibility of the modified electrode

The WB-S La^{3+}/TiO_2-NS/GCE was examined for the reproducibility by studying the current behavior of NFT with five electrodes constructed by the same ways. According to the findings, the relative standard deviation (RSD) of the electrodes was 2.83% for NFT. The WB-S La^{3+}/TiO_2-NS/GCE was also examined for the stability to NFT during four weeks. There was a reduction in the currents responses by 2.41% for NFT. Accordingly, the as-developed WB-S La^{3+}/TiO_2-NS/GCE possessed a commendable reproducibility long stability for sensing NFT, so that it can show analytical application for detection of the NFT for over one month with no noticeable influence in its activity.

Interference analysis

We evaluated the impacts of possible interferants present in bio-fluids or pharmaceutical formulations for concurrent detection of 10.0 µM of NFT. The greatest level of the possible interferants, which causes an error of <5%, was regarded as the tolerance limit. According to the findings, 1000 times the level of glucose, phenylalanine, alanine, sucrose and methionine, and 500 times the content of histidine and glycine had no impact on the NFT reduction currents, underlining the successful performance of the as-fabricated sensor for concurrent detection of NFT.

Real sample testing

Therefore, we employed the standard addition method for evaluating the potential of the WB-S La^{3+}/TiO_2-NS/GCE as one of the novel analytical approaches to determine NFT in the real samples (Table 1). According to the table, the recoveries from 98.6 to 102.0% verified the major ability of the WB-S La^{3+}/TiO_2-NS/GCE as one of the modern nanosensors to detect NFT in the real samples.

Table 1. Determination of NFT in NFT tablets, human blood serum and urine samples. All the concentrations are in μM (n=5).

Sample	Spiked	Found	Recovery (%)	R.S.D. (%)
NFT tablets	0.0	3.8	-	2.4
	5.0	8.7	98.9	2.8
	10.0	13.8	100.7	3.1
Human blood serum	0.0	0.0	-	-
	5.0	5.1	102.0	1.6
	10.0	9.9	99.0	2.2
Urine	0.0	0.0	-	-
	15.0	14.8	98.6	2.7
	25.0	25.1	100.4	1.7

Comparison of the introduced approach and the literature approaches

As shown, a comparison between the WB-S La^{3+}/TiO^2-NS/GCE analytical function developed in the present investigation and additional sensors included in the NFT analyses has been shown in Table 2 [28,29-31]. Regarding earlier published techniques in the publications, it can be concluded that the recommended approach is inferior concerning the detection limit. The advantage of the present study was determining NFT in an extended linear dynamic spectrum (0.001-500.0 μM), considerable sensitiveness and very good stability in comparison with other techniques. This implies that WB-S La^{3+}/TiO^2-NS/GCE owns advantageous analytical performance for NFT determination regarding extended linear dynamic spectrum, high repeatability, a remarkably low detection limit, reproducibility, and also considerable sensitiveness in comparison with published approaches.

Table 2. Comparison between various electroanalytical methods for the determination of NFT with the proposed method.

Method	Modified electrode	LOD	Linear working range	Ref.
Voltammetry	$BaSnO_3$/GCE	0.062 μM	0.01-557.65 μM	[28]
Voltammetry	$ZnCo_2O_4$ NS/GCE	0.013 μM	0.05-10.0 μM	[29]
Voltammetry	Ag/$Ni(OH)_2$/GCE	0.079 μM	0.11-212.0 μM	[30]
Voltammetry	La_2YBiO_6/MWCNTs/GCE	13.74 nM	10.0-120.0 nM	[31]
Voltammetry	WB-S La^{3+}/TiO_2-NS/GCE	0.57 nM	0.001-500.0 μM	This work

Conclusion

The detection sensitivity of WB-S La^{3+}/TiO_2-NS/GCE were shown in NFT electrochemical analysis, the results of which indicated that NFT was easily oxidized on the electrode with reduction potential of 0.45 V. The anchoring of WB-S La^{3+}/TiO_2-NS on the glassy carbon electrode boosted the electron transfer between the electrode surface and the NFT and the peak current. The limit of detection was as low as the 0.57 nM using the modified electrode. Moreover, the proposed sensor was successful in sensing the NFT in real specimens, and exhibited appreciable stability and repeatability.

References

1. Vinothkumar V, Kesavan G, Chenm SM. Graphitic carbon nitride nanosheets incorporated with polypyrrole nanocomposite: A sensitive metal-free electrocatalyst for determination of antibiotic drug nitrofurantoin. Colloids and Surfaces A. 2021;629:127433.

2. Hammam E. Determination of nitrofurantoin drug in pharmaceutical formulation and biological fluids by square-wave cathodic adsorptive stripping voltammetry. Journal of Pharmaceutical and Biomedical Analysis. 2002;30:651-659.

3. Sidar AR, Ahmad M, Siddiqui KA. Synthesis of hydrogen bonded copper (II) coordination polymer: Photocatalytic degradation of Rose Bengal dye and luminescent sensing of Hg^{+2}, $Cr_2O_7^{2-}$, and nitrofurantoin. Polyhedron. 2023;244:116605.

4. Li M, Zhe T, Li R, Bai F, Jia P, Xu Z, Wang X, Bu T, Wu H, Wang L. ZIF-derived Co nanoparticles embedded into N-doped carbon nanotube composites for highly efficient electrochemical detection of nitrofurantoin in food. Food Chemistry. 2023;418:135948.

5. Cai Z, Pang S, Wu L, Hao F, Rong J. Highly sensitive and selective fluorescence sensing of nitrofurantoin based on water-soluble copper nanoclusters. Spectrochimica Acta A. 2021;255:119737.

6. Li M, Zhe T, Li F, Li R, Bai F, Jia P, Bu T, Xu Z, Wang L. Hybrid structures of cobalt-molybdenum bimetallic oxide embedded in flower-like molybdenum disulfide for sensitive detection of the antibiotic drug nitrofurantoin. Journal of Hazardous Materials. 2022;435: 129059.

7. Pacholak A, Juzwa W, Zgoła-Grześkowiak A, Kaczorek E. Multi-faceted analysis of bacterial transformation of nitrofurantoin. Science of the Total Environment. 2022;874:162422.

8. Harrison J, Lewis DA, Ancill RJ. The spectrophotometric determination of nitrofurantoin in blood and urine. Analyst. 1973;98:146.

9. Aufrere MB, Hoener B, Vore ME. High-performance liquid-chromatographic assay for nitrofurantoin in plasma and urine. Clinical Chemistry. 1977;23:2207-2212.

10. Liu W, Zhao C, Zhang Y, Lu S, Liu J, Xi R. Preparation of Polyclonal Antibodies to a Derivative of 1-Aminohydantoin (AHD) and Development of an Indirect Competitive ELISA for the Detection of Nitrofurantoin Residue in Water. Journal of Agricultural Food Chemistry. 2007;55:6829-6834.

11. Patel DS, Sharma N, Patel MC, Patel BN, Shrivastav PS, Sanyal M. Quantitation of nitrofurantoin in human plasma by liquid chromatography tandem mass spectrometry. Acta Pharmaceutica. 2013;63:141-158.

12. Zhang Y, Zhao D, Liu Z, Yang J, Niu X, Fan L, Hu T. Synthesis of two isostructural Zn-CPs and their fluorescence sensing for Cr (VI) ion and nitrofurantoin in aqueous medium. Journal of Solid State Chemistry. 2020;282:121086.

13. Wilasinee D, Sutthivaiyakit P, Sutthivaiyakit S. Determination of Nitrofurans in Chicken Feed by High-Performance Liquid Chromatography–Tandem Mass Spectrometry. Analytical Letters. 1979;48:1979-1987.

14. Zhang F, Yao H, Chu TU, Zhang G, Wang Y, Yang Y. A lanthanide MOF thin-film fixed with Co_3O_4 nano-anchors as a highly efficient luminescent sensor for nitrofuran antibiotics. Chemistry – A European Journal. 2017;23:10293-10300.

15. Omidinejad M, Alimoradi M, Ramezani M, Ebrahimi S. The Electrochemical Sensor for Selective Solid Phase Extraction of Pseudoephedrine Hydrochloride in a Real Sample. Journal of Applied Chemical Research. 2021;15:8-23.

16. Jahani Sh, Sedighi A, Toolabi A, Foroughi MM. Development and characterization of La_2O_3 nanoparticles@snowflake-like Cu_2S nanostructure composite modified electrode and application for simultaneous detection of catechol, hydroquinone and resorcinol as an electrochemical sensor. Electrochimica Acta. 2022;416:140261.

17. Kia S. Electroanalytical Sensor Based on Molecularly Imprinted Polymer-Modified Screen-Printed Carbon Electrode for the Determination of Thyroxine. Journal of Applied Chemical Research. 2023;17:41.

18. Iranmanesh T, Jahani Sh, Foroughi MM, Shahidi Zandi M, Hasani Nadiki H. Synthesis of La_2O_3/MWCNT nanocomposite as the sensing element for electrochemical determination of theophylline. Analytical Methods. 2020;12:4319-4326.

19. Firouzi M, Najafi M. Mesalazine Modified Carbon Paste Electrode for Voltammetric Determination of Amlodipine. Journal of Applied Chemical Research. 2023;17:82-95.

20. Wu J, Luo Y, Qin Z. Composite-modified nano-TiO_2 for the degradation of automobile exhaust in tunnels. Construction and Building Materials. 2023;408:133805.

21. Zhang X, Zhang X, Wang B, Lan L, Yang H, Wang Z, Chang X, Wang S, Ma X, Qiao H, Lin H, Han S, Huang Y. Synergistic effects of lanthanum and strontium to enhance the osteogenic activity of TiO_2 nanotube biological interface. Ceramics International. 2020;46:13969-13979.

22. Babakhani A, AzamiGheimasi S. Preparing self-cleaning and antibacterial polysulfone nano-fibers using TiO_2, ZnO, and SiO_2 nanoparticles with electrospinning method. Invention Disclosure. 2023;3:100015.

23. Verma V, Singh SV. Augmentation of photocatalytic degradation of methylene blue dye using lanthanum and iodine Co-doped TiO_2 nanoparticles, their regeneration and reuse; and preliminary phytotoxicity studies for potential use of treated water. Journal of Environmental Chemical Engineering. 2023;11:111339.

24. Gu K, Chen B, Chen Y. Preparation and tribological properties of lanthanum-doped TiO_2 nanoparticles in rapeseed oil. Journal of Rare Earths. 2013;31:589-594.

25. Wang Q, Xu S, Shen F. Preparation and characterization of TiO2 photocatalysts co-doped with iron (III) and lanthanum for the degradation of organic pollutants. Applied Surface Science. 2011;257:7671-7677.

26. Liu J, Li X. Hydrothermal synthesis of CdTe quantum dots–TiO_2–graphene hybrid. Physics Letters A. 2014;378:405-407.

27. Bard AJ. Faulkner LR. Electrochemical Methods: Fundamentals and Applications. 2001; second ed., Wiley, New York.

28. Balamurugan M, Alagumalai K, Chen TW, Chen SM, Liu X, Selvaganapathy M. Simultaneous electrochemical determination of nitrofurantoin and nifedipine with assistance of needle-shaped perovskite structure: barium stannate fabricated glassy carbon electrode. Microchimica Acta. 2021;188:1-13.

29. Koventhan C, Vinothkumar V, Chen SM, Sangili A, Highly sensitive electrode materials for voltammetric determination of nitrofurantoin based zinc cobaltate nanosheet. New J. Chem. 2020;44:12036-12047.

30. Ezazi M, Asadpour-Zeynali K, Saeb E, Synergistic incorporation of Ag into nickel hydroxide nanostructure to enhance the electroctrocatalytic determination of nitrofurantoin. Inorg. Chem. Commun. 2024;160:111913.

31. Ravikumar SB, Prasanna SB, Shivamurthy SA, Shadakshari S, Nagaraja BM, Rajabathar JR. Arokiyaraj S, Individual and simultaneous electrochemical determination of nitrofurantoin and ascorbic acid in biological samples using a novel La_2YBiO_6 double perovskite deposited on MWCNTs as a nanocomposite. New J. Chem. 2023; 47: 21307-21317.